Sumerianz Journal of Scientific Research, 2023, Vol. 6, No. 2, pp. 33-39
ISSN(e): 2617-6955, ISSN(p): 2617-765X
Website: https://www.sumerianz.com
DOI: https://doi.org/10.47752/sjsr.62.33.39

Original Article Open Access

A New CT Construction System Suitable for Micro- and Macro-Focal Beam Guides Using a Multitarget System

W. Ulmer
Gesellschaft für Qualitätssicherung in der Medizin, Deizisau, Germany
Email: waldemar.ulmer@gmx.net

Article History

Received: 13 April 2023

Revised: 10 June 2023

Accepted: 18 June 2023

Published: 25 June 2023

How to Cite

W. Ulmer., 2023. "A New CT Construction System Suitable for Micro- and Macro-Focal Beam Guides Using a Multitarget System ". *Sumerianz Journal of Scientific Research*. Vol. 6, pp. 33-39.

Abstract

The goal of this study is the improvement of CT constructions by exploiting the Bremsstrahlung created by multitarget systems allowing additional focusing influences by suitable magnetic fields and small-angle scatter of the walls (preferably tungsten). The number of layers of these configurations can be restricted to 10 – 15 layers, if electron voltages are of the order 120 keV – 180 keV, depending on the kind of application (medical CT or CT in the technical/research field). The theoretical results very satisfactorily agree with Monte-Carlo calculations using GEANT4.
Keywords: Bremsstrahlung; Macro-focal beam; Multi-layer targete system; Computed CT scanning.

1. Introduction

Computed CT scanning tomography (see e. g. reviews [1, 2] has reached rather different applications such as diagnostics [3], radiotherapy [4], and material research in the technical domains [5] (e. g. accurate determination of the geometry of probes, material defects and structure elucidation). The purpose of this communication is coupled electrical circuits in quantum theory to calculate Bremsstrahlung of different CT modalities improving scanning by tomography methods [6].

In a short review information on the theoretical means is presented. The physical basis is represented by Figure 1, which shows 2 circuits with magnetic and electric couplings and driving voltages.

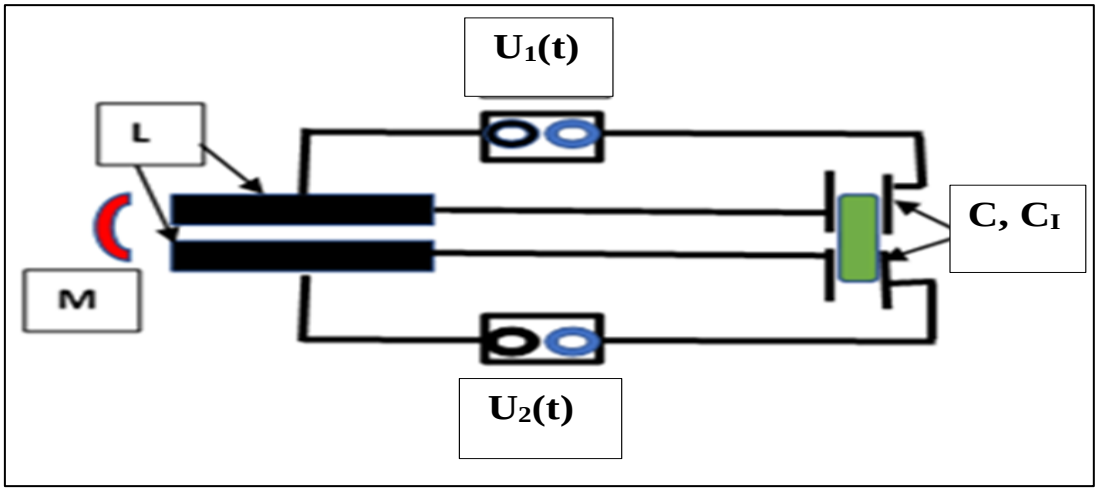

Figure-1. Two circuits with mutual electric and magnetic coupling and two different driven forces $U_1(t)$ and $U_2(t)$. L: Induction, M: Magnetic coupling, C: Common Capacitor, C_I: Electric coupling (negative)

The above Figure represents the physical starting-point with regard to all cases considered in this study. The classical description of the above circuits is given by the following equation 1, well-known equations of coupled electromagnetic circuits, the transition to the quantized treatment inevitably necessary for the calculation of Bremsstrahlung is previously presented [6].

$$\left.\begin{aligned} L\cdot\ddot{Q}_1 + M\cdot\ddot{Q}_2 + \tfrac{1}{C}\cdot Q_1 - \tfrac{C_I}{C}\cdot Q_2 = U_1\cdot e^{i\cdot\omega\cdot t} \\ L\cdot\ddot{Q}_2 + M\cdot\ddot{Q}_1 + \tfrac{1}{C}\cdot Q_2 - \tfrac{C_I}{C}\cdot Q_1 = U_2\cdot e^{i\cdot\omega\cdot t} \end{aligned}\right\} (3) \qquad (1)$$

These definitions important with regard to the resonances of the multi-target are given by:

$q_1 = Q_1+Q_2$, $q_2 = Q_1-Q_2$, $U_{11}(t) = U_1(t) + U_2(t)$, $U_{22}(t) = U_1(t) - U_2(t)$,

$\lambda_1 = L+M$, $\lambda_2 = L - M$, $C_1 = C / (1 - C_I)$, $C_2 = C / (1 + C_I)$. (2)

Referring to the substitutions (2) we should note, that in the absence of the driving forces (e.g., $U_1 = U_2 = 0$) the quantum theoretical treatment is rather easy to handle, since it leads to two coupled based on the canonical momenta

$$P_1 = q_{1*}\,\lambda_1 \text{ and } P_2 = q_{2*}\,\lambda_2. \qquad (3)$$

In eq. (3) a negative capacitive coupling it assumed, yet a positive coupling only requires the substitutions

$C_1 = C/ (1 + C_I)$, $C_2 = C / (1 - C_I)$, and eq. (4) will not be changed.

Thus, according to the previous publication [6] the related Lagrange function £ and Hamiltonian have been developed and solved even for the case of driving forces, which are essential features in the present study, too:

$$\left.\begin{aligned} \pounds = \tfrac{\lambda_1}{2}\cdot\dot{q}_1^2 - \tfrac{1}{2\cdot C_1}\cdot q_1^2 + U_{11}\cdot\lambda_1\cdot e^{i\cdot\omega\cdot t} \\ + \tfrac{\lambda_2}{2}\cdot\dot{q}_2^2 - \tfrac{1}{2\cdot C_2}\cdot q_2^2 + U_{22}\cdot\lambda_2\cdot e^{i\cdot\omega\cdot t} \end{aligned}\right\} (4)$$

This, fact implies that the quantization leads to a time-dependent task of coupled oscillators, e.g., a time-dependent Schrödinger equation. The voltages U_1 and U_2 provide the electron current necessary for the calculation of the quantum yield of the Bremsstrahlung. The eigenfrequencies now assume the shape:

$$\omega_1^2 = 1/(\lambda_1\cdot C_1),\ \omega_2^2 = 1/(\lambda_2\cdot C_2). \quad (5)$$

$$\left.\begin{aligned} H_1 = \tfrac{1}{2\cdot\lambda_1}\cdot P_1^2 + \tfrac{\lambda_1}{2}\cdot\omega_1^2\cdot q_1^2 - q_1\cdot U_{11}\cdot e^{i\cdot\omega\cdot t} \\ H_2 = \tfrac{1}{2\cdot\lambda_2}\cdot P_2^2 + \tfrac{\lambda_2}{2}\cdot\omega_2^2\cdot q_2^2 - q_2\cdot U_{22}\cdot e^{i\cdot\omega\cdot t} \end{aligned}\right\} (6)$$

$$\omega_1^2 = \tfrac{1}{\lambda_1\cdot C_1};\ \omega_2^2 = \tfrac{1}{\lambda_2\cdot C_2} \quad (6a)$$

The solutions of these equations appear to be rather difficult due to the time-depending forces U_1 and U_2. They can be handled by creation - and annihilation operators. Interested readers should consult the paper [6]. In particular, the creation of Bremsstrahlung is immediately connected to these forces.

The time-dependent Schrödinger equation is given by equations (7) and (7a).

$$\left.\begin{aligned} P_k\psi \to \tfrac{\hbar}{i}\tfrac{\partial}{\partial q_k}\psi; \\ \rho_k = U_k\cdot\sqrt{\tfrac{\hbar}{2\cdot\lambda_k\cdot\omega_k}};\ \xi_k^2 = \tfrac{\lambda_k\cdot\omega_k}{\hbar}\cdot q_k^2 \\ k = 1,\ 2;\ U_k = U_{11}\,(k=1);\ U_k = U_{22}\,(k=2) \end{aligned}\right\} (7)$$

$$-\tfrac{1}{2}\tfrac{\partial^2}{\partial\xi_k^2}\psi_k + \tfrac{1}{2}\xi_k^2\psi_k - \rho_k U_k\psi_k = i\cdot\hbar\tfrac{\partial}{\partial t}\psi_k \quad (7a)$$

Therefore, we now pass to the solution results.

1. Creation of Bremsstrahlung by exploiting specific features of the electron beam line.

This chapter refers to the role of the plate thickness in the multitarget system and of the influence of small angle scatter and additional magnetic fields for focusing the beam-line. In order to present a noteworthy example, we consider in Figures 2, 3, 3a, and 5a comparison of a standard target and a multi-target system of a 6 MV linear accelerator, since this represents a well-known configuration with regard to the standard target.

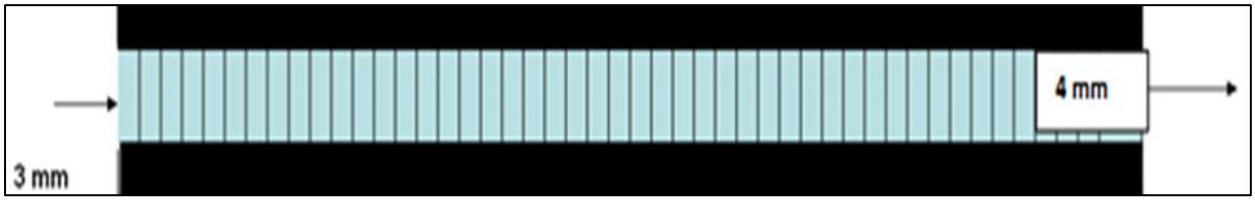

Figure-2. Linear accelerator with a multitarget according to the right-hand side of Figure 3

The Figures below standard consist of standard target (case Figure 3) with one tungsten target (black) and a copper layer for cooling (green). The primary collimator (wight) and the flatness filter (bleu) are further components of this kind of linear accelerator. The multi-layer target (right) consists of 100 plates, thickness of each plate 0.01 mm. The total thickness amounts to 1 mm and agrees with the corresponding thickness of the standard case. A further advantage of a multitarget system is that it works without cooling, since the short path of electrons in these thin plates leads to a very negligible heat production, the outlet belt occurs by the walls.

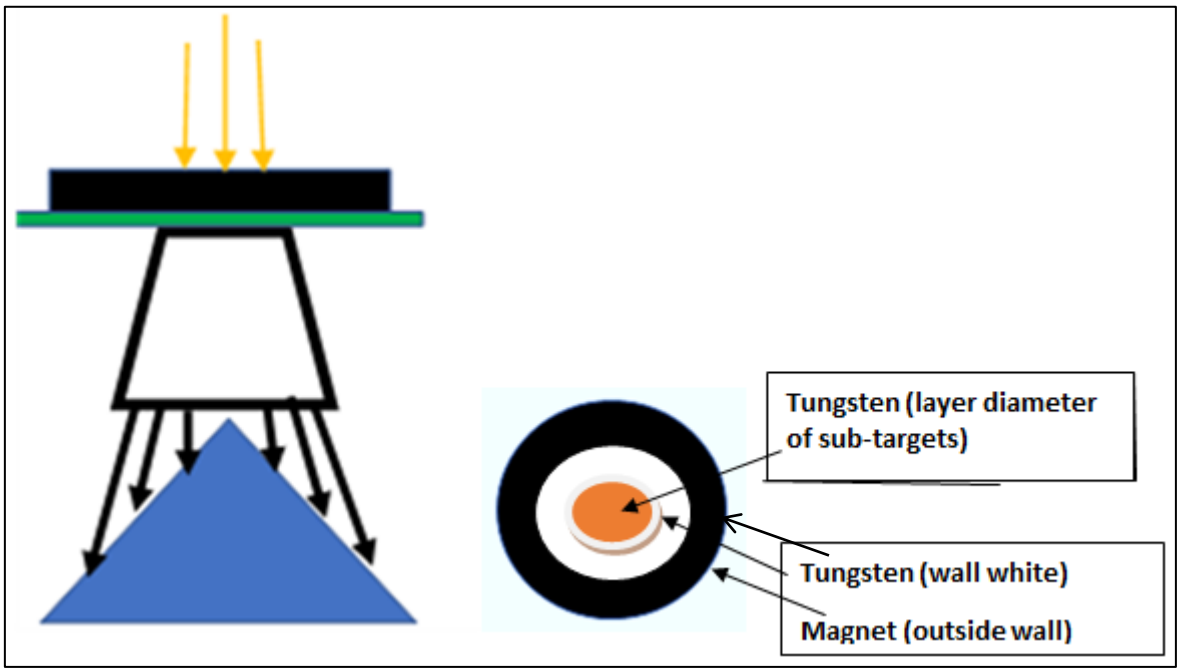

Figure-3. Left: Standard target **Figure-3a.** Right: Top view of a multitarget

The problem of a single target (standard case, right-hand side) and multi-layer target (left-hand side) is shown by the above Figure. In the case of a standard target, lateral and backscatter processes of the impinging electrons prevent the exploitation of small angle scatter, and the increased electron paths lead to additional heat production. Therefore, the property of the one single target (standard target) demonstrates the significant disbenefit in the above case, which can be avoided by a multi-target system.

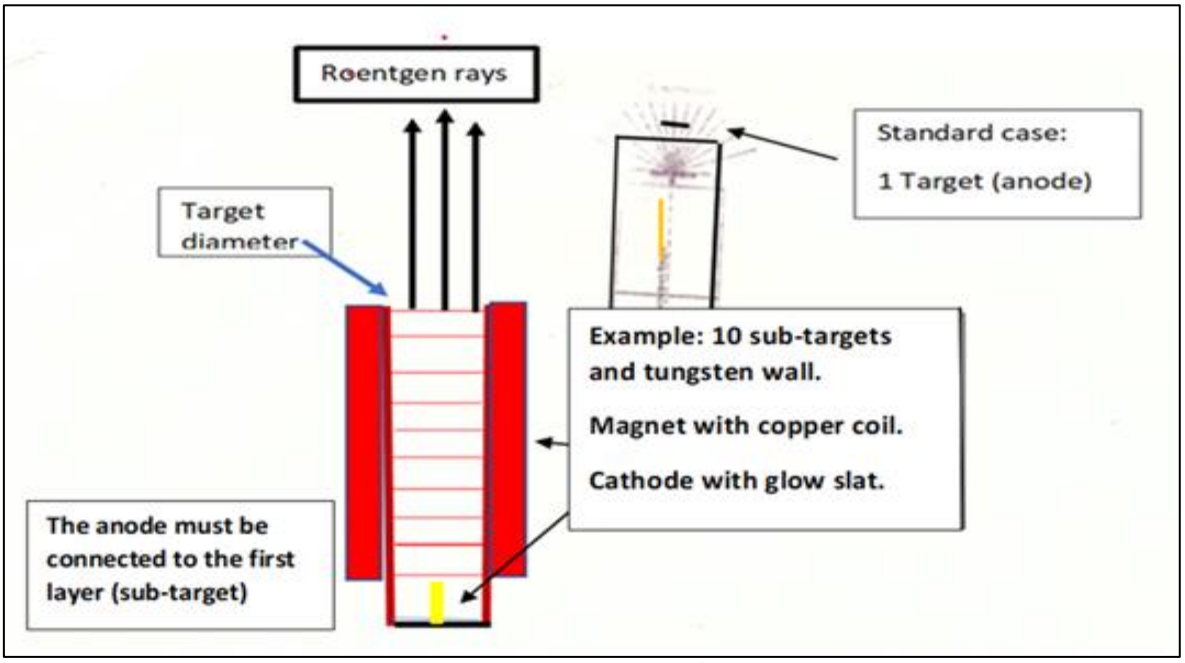

Figure-4. This Figure demonstrates the comparison between the X-ray creation of a multi-target system (10 layers) and the standard target consisting of a single target. The above multi-target can be restricted to a voltage V implying an energy of the impinging electrons to 120 keV. Since each layer has the thickness of 0.012 mm tungsten, the total target thickness amounts to 0.12 mm and the distance between the sub-targets to 0.5 cm

In Figure 5 we are able to point out the requirements of the layer diameter in a multitarget system: The macro-focal diameter can be of the order 1 mm – 4 mm (this is a suitable order for a medical CT), whereas the micro-focal diameter should in every case be < 1 mm. The extension to nano-focal systems additionally requires an increased field strength influencing already the impinging electrons produced by the glow wire. Some examples will be

presented in later Figures. There arises also the question on the physical background of small-angle scatter. Thus, it is the electrostatic repulsion, if the depth of penetration is smaller than total material depth. This effect is amplified by the additional magnetic field.

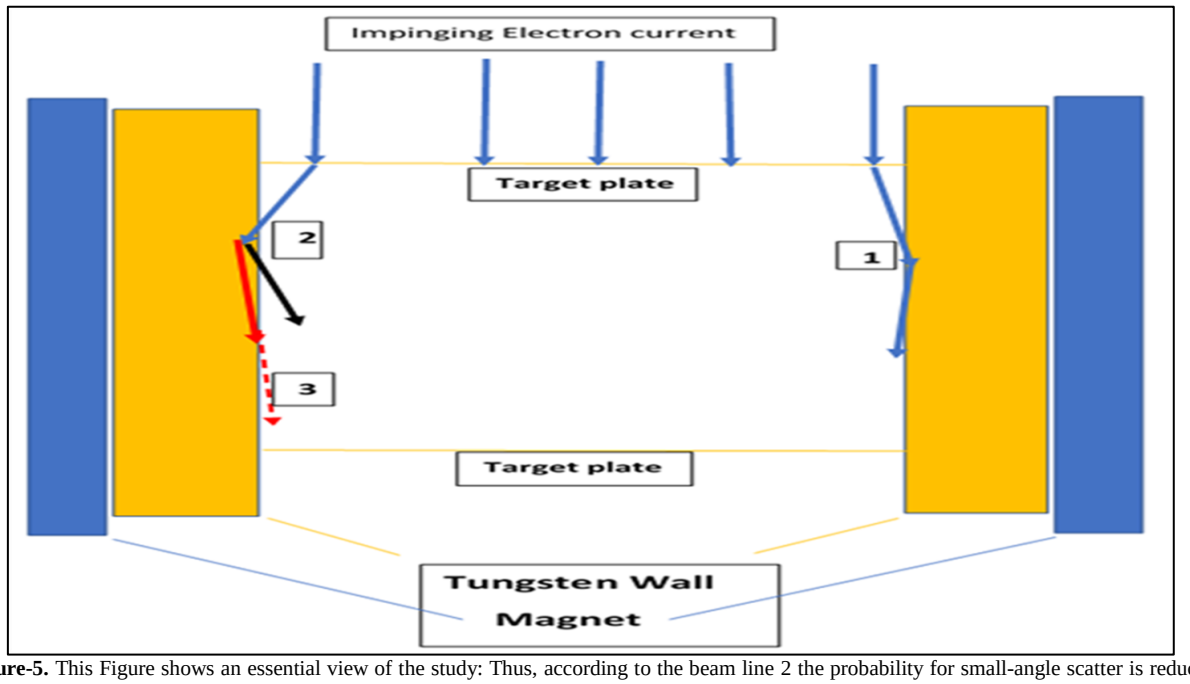

Figure-5. This Figure shows an essential view of the study: Thus, according to the beam line 2 the probability for small-angle scatter is reduced (black arrow), whereas the red dashes (3) incorporate small-angle scatter, too. The impinging beam-line 1 showing a smaller angle increases the probability of small angle-scatter of the impinging electrons

Some detailed properties referring to CT construction of a multi-target system can be verified in Figure 6. The specific arrangement of such a system with tungsten wall and magnet in order to focus the electron beam is shown in Figure 7.

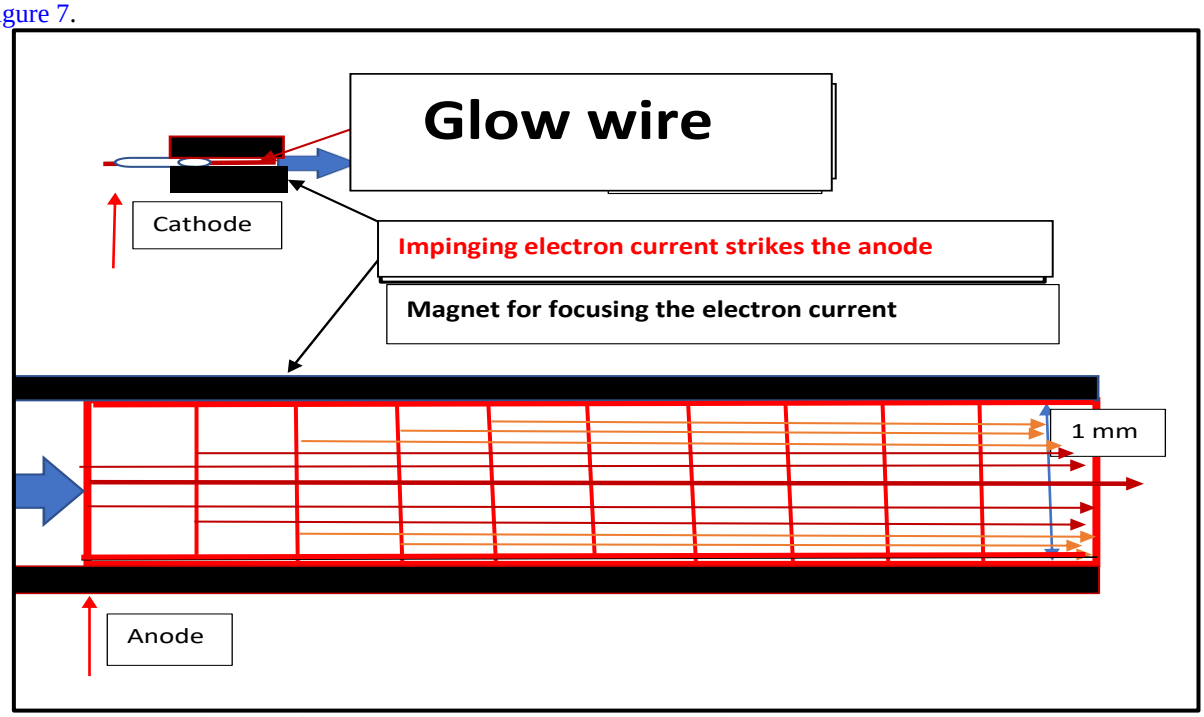

Figure-6. Schematic configuration of a multi-layer CT construction. The thickness of the tube should not exceed about 1 mm for clinical CT or research CT suitable to very small structures and objects. The diameter should not exceed 4 mm. Thus, the consideration of very small objects requires a diameter of about 1 mm. It has also to be pointed out, that the length of the magnet or solenoid have to comprise the electron beam produced at the glow wire in order to reach the requested narrow beam without any losses

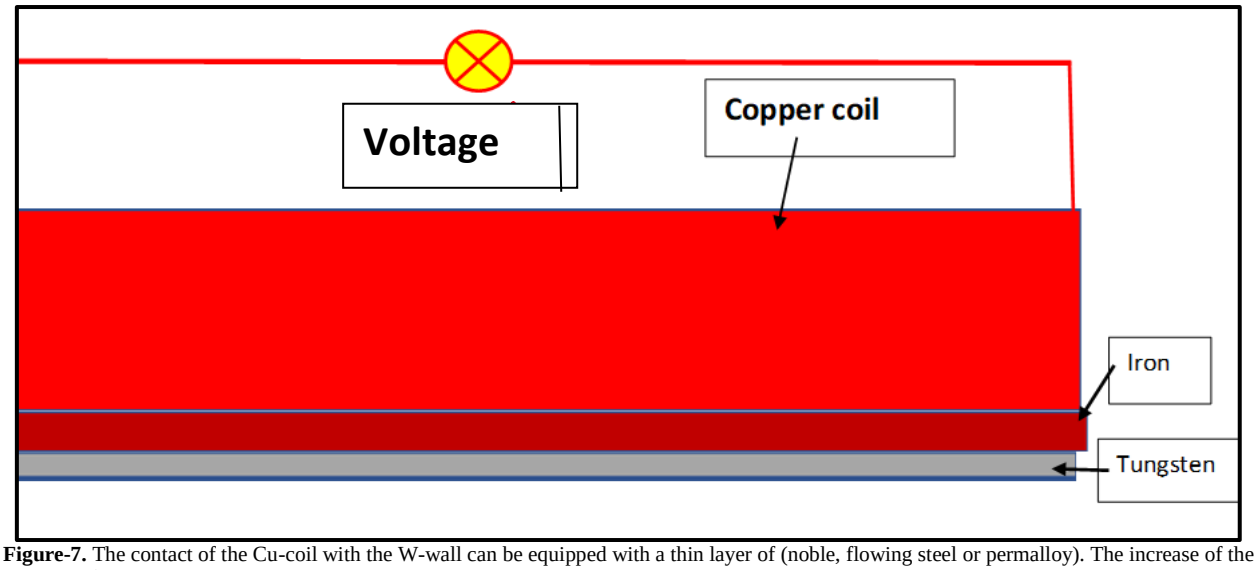

Figure-7. The contact of the Cu-coil with the W-wall can be equipped with a thin layer of (noble, flowing steel or permalloy). The increase of the magnetic field strength can be reached by this way. By that, the electric current can be limited to 2 Ampere or less depending on the used permeability

.

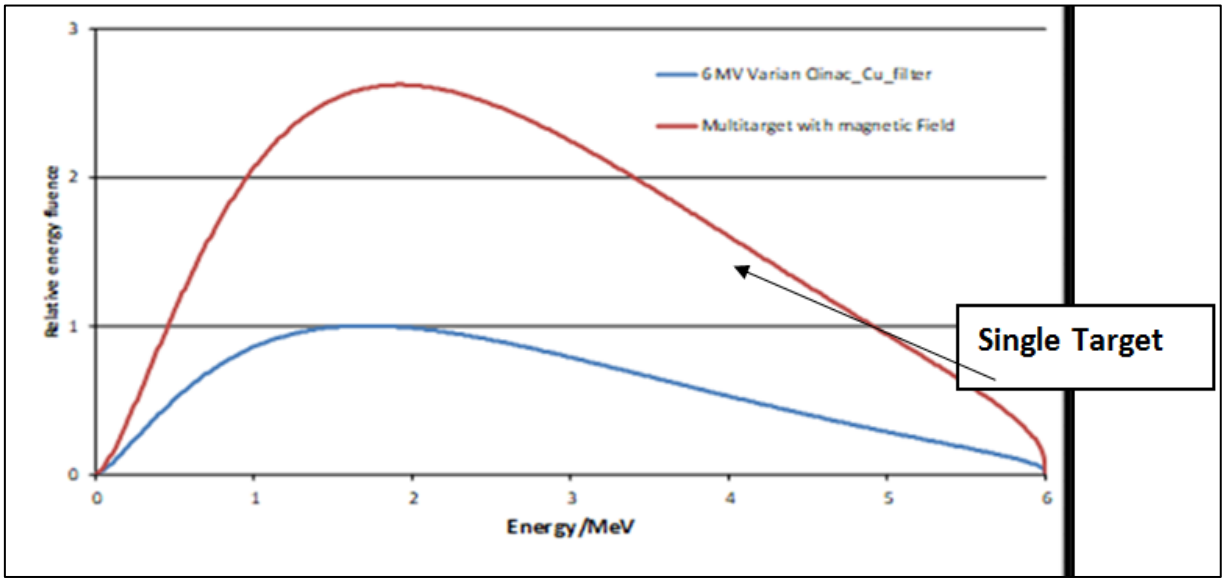

Figure-8. This Figure shows the differences in the energy fluence of a multi-target versus standard target and is referred to 6 MV photons. The total thickness amounts to 1 mm in both cases, and the field size is fixed to 4 x 4 mm^2. It should be pointed out, that the red curve is only created by small-angle scatter at the tungsten wall without an additional magnetic field.

In the above case of linear accelerators (Figure 3a) the difficulty is obvious, that the construction of a multi-target system represents a non-negligible task due to the distances between the plates amount to 1 mm. These distances may also be increased to 2 mm, but the manipulation may remain still difficult. It should be added that the blue curve of Figure 8 results from Monte-Carlo calculations using the GEANT4 code [7]. The red curve (multi-target) results from the theoretical method worked out in the previous paper [6]. However, the additional Monte-Carlo calculation (GEANT4) provided only maximal deviations of 0.5 % in order to guarantee the reliability of the theoretical method.

Only the multi-target system is able to exploit small angle scatter of the electron beam line and leads to an increased contribution to the energy fluence (red curve of the above Figure), whereas the blue curve corresponds to the case according to Figure 3. This fact is a clear indication, that the standard target can be characterized has to be related to heat production by multiple scatter production

Table 1 provides the significant hint, that, above all, tungsten (W) is able to provide the desired all necessary properties of a multi-target system.

Table-1. Important material properties

	Electron affinity	**Conductivity**	**Heat conductivity**
Element	eV	A·V-1·m-1	W·m-1K-1
Cu	4,65	58,1·106	400
W	4,55	18,52·106	170
Ta	4,19	7,68·106	57
Pt	5,65	9,48·106	72

Thus, besides tungsten (W) one may account for tantalum (Ta) due to its easier manipulation. However, the heat conduction is small. There are the following properties of interest: Density of Ta^{181}_{73} = 16.65 g/cm^3, ratio of nuclear charge and nuclear mass: 73/181 = 0.403315; density of W^{184}_{74} = 19.25 g/cm^3, ratio of nuclear charge and nuclear mass: 74/184 = 0.402174.

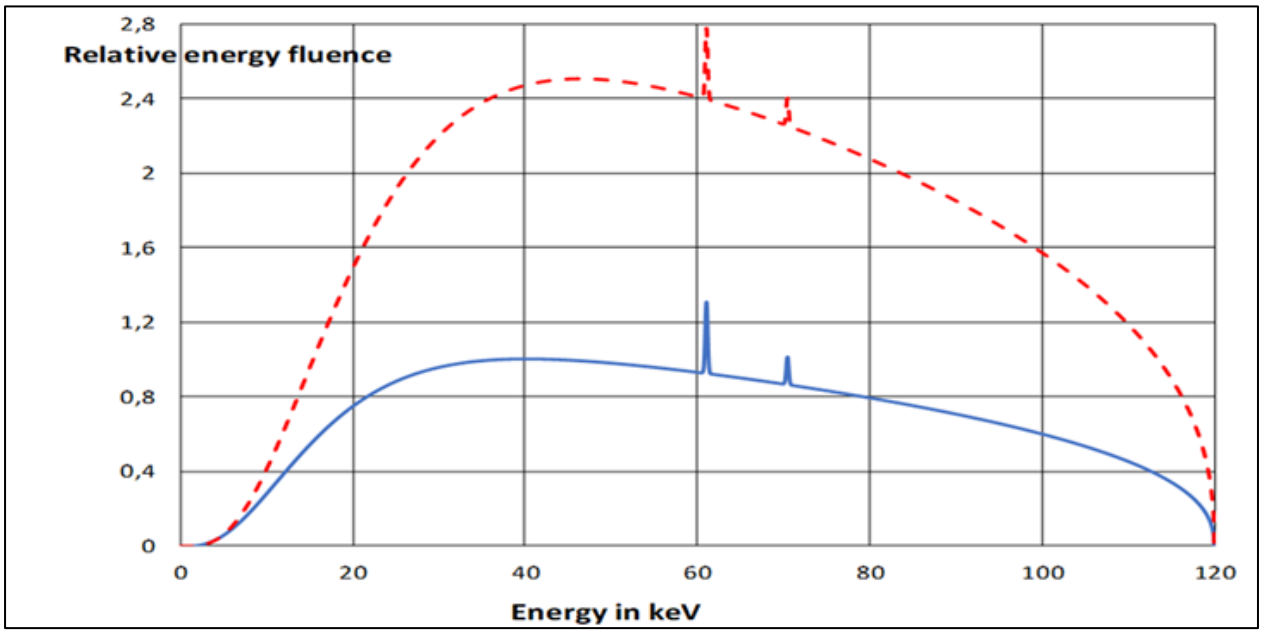

Figure-9. This Figure shows the energy fluence distribution of a multi-target system consisting of 10 layers (red curve, magnetic field strength: 0.5 T) and of a standard target according to Figure 3

This Figure can be associated to usual CT configuration properties, necessary to medical applications in the clinical routine. In particular, the distance between the layers now can amount to 0.5 cm, and the ten layers are sufficient. Figures 10 and 11 present multi-target systems with more than 10 layers and raised magnetic field strengths.

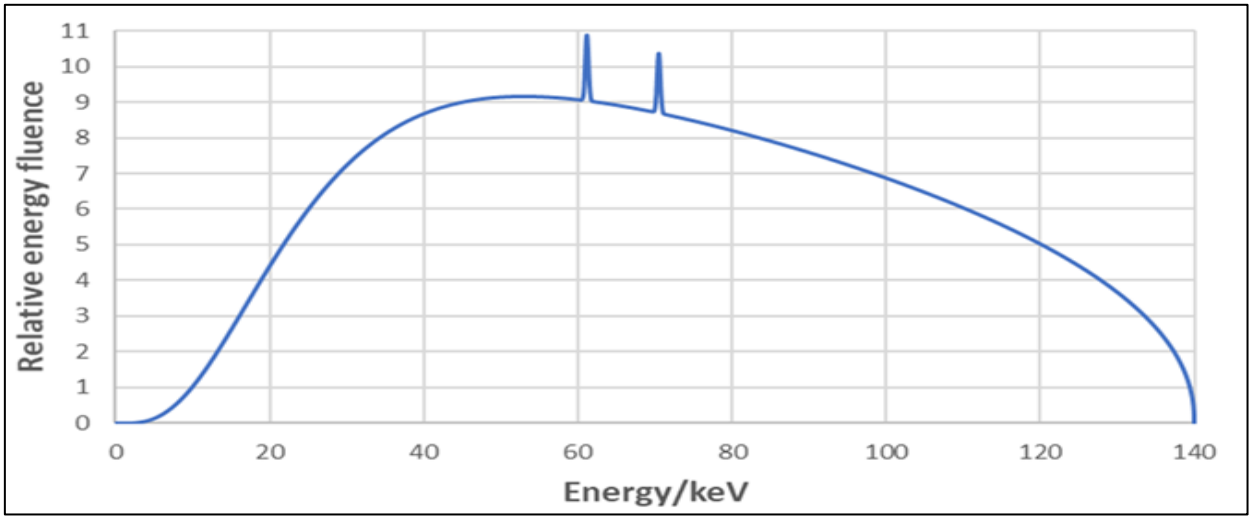

Figure-10. This Figure presents a possible multi-target CT construction with 12 layers and 1 T magnetic field strength. The diameter of each layer amounts to 1 mm, and the distance between the layers to 5 mm. The discrete resonance peaks of tungsten at 61.12 keV and 70.41 keV are noteworthy features in this and in the Figures 9 and 11. The different energy fluences of this Figure and those of Figures 9 can be verified

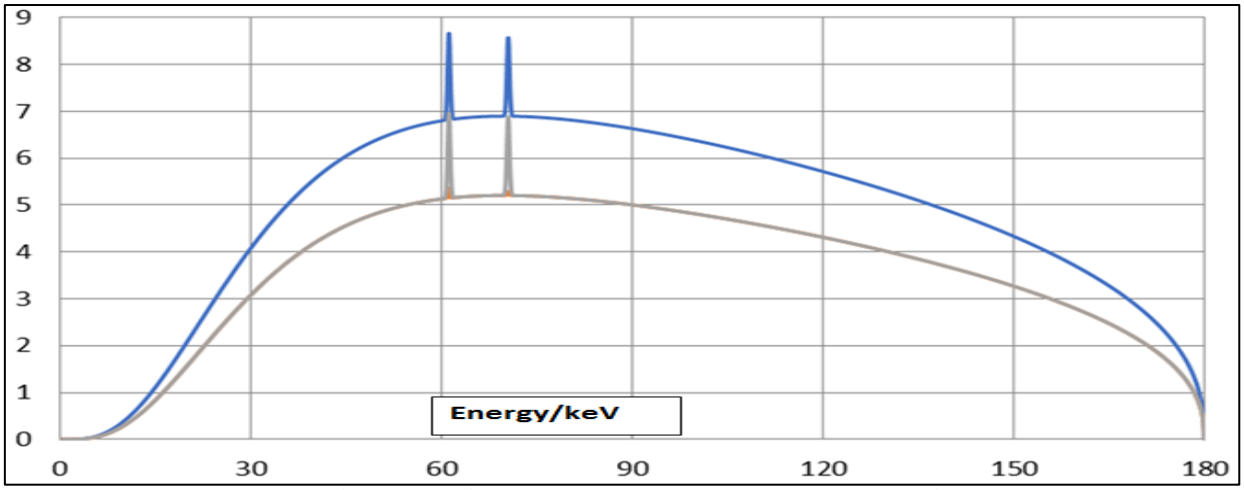

Figure-11. The role of the magnetic field strength in Figure 11 and an increased diameter of the plates (4 mm)

A comparison between Figure 10 and 10 appears to be indicated. Thus, the main difference between the two Figures is the diameter of the sub-targets, 1 mm in Figure 10, and 4 mm in Figure 11, and the increased magnetic field strength in Figure 10. By that, it would be necessary to restrict the diameter of sub-targets in Figure 11, too, to 1 mm or << 1 mm, and a higher magnetic field strength, in order to be suitable for micro- order nano- technology, i.e., greater than 1 T.

2. Conclusions

The advantages of multi-layer targets are the following facts:

Avoidance of additional cooling with copper, and a reduction of the electric current by exploitation of small angle scatter. Conventional CT constructions are less efficient by later- and backscatter. The higher the voltage of the accelerated electrons, the number of layers should also be increased. Since usual medical applications work with 120 keV and 140 keV, the CT constructions are less intricate. It should be noted, that the multi-layer configurations need radiation transmission emitters, as also true for conventional CT. The magnetic field strength can significantly be amplified by suitable permeabilities like flow steel, which amounts to about 4000 and permalloy even to 300000. Thus, the current supply could be drastically reduced.

The disadvantage of a multi-target system is the increased effort with respect to its production. However, it should be mentioned, that the use of tantalum is easier to handle than tungsten, but the distance between the layers of 0.5 cm and the restriction to 10 – 15 plates make the handling with tungsten acceptable compared with the case shown in Figure 2 for linear accelerators.

It should finally be added, that all curves of the above Figures have been checked by GEANT4 [7]. Thus, the deviations with respect to the theoretical calculations developed previously [6] at the most amounted to 0.5 %. Therefore, a further, separate verification appears to be not necessary.

References

[1] Mikla, V. I. and Mikla, V. V., 2014. "Computed tomography." *Medical Imaging Technology*, Available: https://doi.org/10.1016/B978-0-12-417021-6.00002-2

[2] Schioppa, E. J., Uher, J., and Visser, J., 2012. "Construction and test of an X-ray CT setup for material resolved 3D imaging with Medipix based detectors." *Journal of Instrumentation*, vol. 7, p. C10007.

[3] Buzug, T. M., 2008. *Computed tomography*. Berlin Heidelberg: Springer.

[4] Varian Radiation planning with Eclipse (IMRT VMAT), 2022. "Varian user manual~."

[5] Christoph, R. and Neumann, H. J., 2011. *Roentegen-tomography in der industriellen messtechnik*. München: Verlag Moderne Industrie.

[6] Ulmer, W., 2021. "The role of forced oscillators of coupled circuits in radiation physics – new linear accelerator design improving tomography technology (radiotherapy and ct), heisenberg-euler scatter, and extension to 'bremsstrahlung' with gev electrons." *J. of Applied Mathematics and Physics*, vol. 9, pp. 707-735.

[7] GEANT4, 2020. "User manual edited by the CERN-library."